Title of paper:

AN ANALYTICAL SOLUTION FOR THE CONSOLIDATION AROUND A LATERALLY LOADED PILE

Ashraf S. Osman
Lecturer,
School of Engineering,
Durham University,
South Road,
Durham DH1 3LE, UK
Tel: +44 191 334 2388;
Fax: +44 191 334 2390;
E-mail: ashraf.osman@durham.ac.uk

Mark F. Randolph
ARC Federation Fellow and Professor of Civil Engineering,
Centre for Offshore Foundation Systems,
University of Western Australia,
Perth, WA6009, Australia
Phone: (61 8) 6488 3075
Fax: (61 8) 6488 1044
E-mail: randolph@civil.uwa.edu.au

ABSTRACT

This paper presents a closed-form analytical solution for the consolidation of the soil around a laterally loaded pile, assuming the soil skeleton deforms elastically and under plane strain conditions. The problem is idealised as a circular rigid disc surrounded by a deformable soil zone. Expressions for the initial excess pore water pressure distribution are derived from the mean total stress changes given by the elastic solution. Curves showing decay of the excess pore water pressure with time, and also the variation of pile displacement, are plotted in non-dimensional form. The parameters that affect the displacement prediction are illustrated and discussed.

INTRODUCTION

The problem of the response of a single cylindrical pile embedded in a homogeneous elastic soil and subjected to lateral load has received the attention of many researchers. Winkler's (1867) concept of the modulus of sub-grade reaction has often been used to evaluate lateral displacements. In this approach the pile is regarded as a beam resting on elastic supports and the soil reaction is assumed to be proportional to deflection occurring at the point in question. The coefficient of proportionality was termed the coefficient of subgrade reaction, expressed as the ratio of average pressure across the width of the pile to the deflection (thus with dimensions of pressure divided by length). More recent work adopts the 'subgrade modulus' as the ratio of force per unit length along the pile to the lateral deflection (dimensions of modulus, or force per length squared), The latter approach is more useful as the subgrade modulus is similar, both in dimensions and value, to the Young's modulus, E of the soil. Several modifications of this general approach can be found in the literature (Hetenyi, 1946, Matlock & Reese, 1960, Mylonakis, 2001)

Poulos (1971) used an alternative approach to provide a general solution to the problem in a homogeneous linear and isotropic elastic medium by comparing the pile to a thin plate, using Mindlin's formulae (1936) to determine soil displacements. Randolph (1981) presented algebraic expressions which allow the behaviour of flexible piles under lateral loading to be calculated, in terms of fundamental soil properties. These expressions are based on the results of finite element studies of the response of a laterally loaded cylindrical pile embedded in elastic soil with stiffness varying linearly with depth.

Baguelin et al. (1977) developed analytical solutions for the problem of a section of the elastic-plastic soil-pile system, assuming plane strain conditions. The plane-strain simplification is justified, at least near the pile, because the displacements of the various sections of the pile vary in a continuous manner. The analytical solution required an assumption that the displacements vanished at a distance R away from a rigid disc representing a pile of radius r_o (Figure 1), without which infinite displacements would result. The solution was derived from a single Airy stress function expressed in polar coordinates (r, θ). Assuming the pile is bonded to an intact elastic soil, expressions for stress changes in the soil around the pile are:

$$\sigma_r = \frac{F}{4\pi r_0}\frac{1}{(1-\nu)}\left[(3-2\nu)\frac{r_0}{r} - \frac{1}{1+(r_0/R)^2}\left(\frac{r_0}{r}\right)^3 + \frac{1}{(3-4\nu)}\frac{1}{1+(R/r_0)^2}\frac{r}{r_0}\right]\cos\theta \qquad (1)$$

$$\sigma_\theta = -\frac{F}{4\pi r_0}\frac{1}{(1-\nu)}\left[(1-2\nu)\frac{r_0}{r} - \frac{1}{1+(r_0/R)^2}\left(\frac{r_0}{r}\right)^3 - \frac{3}{(3-4\nu)}\frac{1}{1+(R/r_0)^2}\frac{r}{r_0}\right]\cos\theta \qquad (2)$$

$$\tau_{r\theta} = -\frac{F}{4\pi r_0}\frac{1}{(1-\nu)}\left[(1-2\nu)\frac{r_0}{r} + \frac{1}{1+(r_0/R)^2}\left(\frac{r_0}{r}\right)^3 - \frac{1}{(3-4\nu)}\frac{1}{1+(R/r_0)^2}\frac{r}{r_0}\right]\sin\theta$$

(3)

where F is the lateral force per unit length, and r_0 is the radius of the pile. The corresponding radial displacement is given by:

$$\rho_r = \frac{F}{16\pi G}\frac{1}{1-\nu}\left[(3-4\nu)\ln\left(\frac{R}{r}\right)^2 - \left(\frac{r_0}{r}\right)^2\frac{R^2-r^2}{R^2+r_0^2} - \frac{(4\nu-1)}{(3-4\nu)}\frac{R^2-r^2}{R^2+r_0^2}\right]\cos\theta \qquad (4)$$

where G is the shear modulus of the soil and ν is Poisson ratio. Baguelin et al. (1977) also developed solutions that take into account the disturbance of the soil in the vicinity of the pile. Expressions relating R to the embedded length of the pile were suggested for different pile head fixity conditions.

In all the above solutions, no consideration was given to the excess pore water pressure that would be generated if the piles are embedded in a saturated load. The initial displacements would then be limited to those corresponding to $\nu = 0.5$, while dissipation of pore water pressure with time would cause additional deformations as the effective stresses increased. Finite element approximation can be used to predict the variation of displacements and stresses with time (Carter and Booker, 1981). Shirazi and Selvadurai (2005) developed a continuum-based computational model for stiff cylinders embedded in damage-susceptible poroelastic material. Osman and Randolph (2010) studied the consolidation around a rigid infinite cylinder and derived expressions for the pore fluid pressure, stresses and displacements in the Laplace domain. However, no closed-form analytical solution in the time-domain has been developed for consolidation around laterally loaded piles.

This paper presents a closed-form analytical solution for the consolidation around a laterally loaded stiff pile embedded in a linear-elastic porous material. Similar to the assumptions used in Baguelin's solutions, a plane strain section of the soil-pile system is considered. The plane strain disc is taken to deform as a rigid body, so its diameter does not change. The excess pore water pressure and the pore water pressure are assumed to

vanish at an outer radius R (Figure 1). It should be noted that soil response is generally nonlinear even at small strain levels. However, a poroelastic model, with the assumption of linear elasticity, is the common starting point for many (if not most) closed form solutions for consolidation problems. They have been shown to give good approximations for the consolidation behaviour (see for example Randolph and Wroth, 1979 and Krost et al., 2010).

The solution presented in this paper is also relevant to other engineering applications such as for consolidation around a T-bar full-flow penetrometer used for in situ testing of soil, and around deeply embedded pipelines.

DERIVATION OF EQUATION FOR PORE WATER PRESSURE DISSIPATION

The equations governing the consolidation of fully saturated porous elastic soil under one-dimensional may be attributed to Terzaghi (1923). These equations were extended by Biot (1941) to cover the general three-dimensional situations. The relation between the variation of the volumetric strain ε_v with time and the excess pore water pressure u_e can be expressed by:

$$\frac{\partial \varepsilon_v}{\partial t} = -\frac{k}{\gamma_w} \nabla^2 u_e \tag{5}$$

where

$\nabla^2 = \frac{\partial^2}{\partial r^2} + \frac{1}{r}\frac{\partial}{\partial r} + \frac{1}{r^2}\frac{\partial^2}{\partial \theta^2}$ in polar coordinates

k is the permeability coefficient, and γ_w is the unit weight of water.

Following the traditional sign convention in soil mechanics, with compressive stresses and strains positive, the radial and circumferential strains for plane strain deformations can be expressed as:

$$\varepsilon_r = \frac{1}{2G}\left[(1-\nu)\sigma'_r - \nu\sigma'_\theta\right] \tag{6}$$

$$\varepsilon_\theta = \frac{1}{2G}\left[(1-\nu)\sigma'_\theta - \nu\sigma'_r\right] \tag{7}$$

where σ_r' and σ_θ' are the (changes in) effective stresses in the radial and circumferential direction respectively. The volumetric strain can therefore be expressed as:

$$\varepsilon_v = \varepsilon_r + \varepsilon_\theta = \frac{(1-2\nu)}{2G}\left(\sigma'_r + \sigma'_\theta\right) = \frac{(1-2\nu)}{G}s' \tag{8}$$

where s' is the mean effective stress change, equal to $(\sigma'_r + \sigma'_\theta)/2$.

Under undrained conditions, volumetric strains are zero and so the initial change in mean effective stress, s', is also zero. Hence the initial excess pore pressure, u_0, is equal to the mean total stress change. From equations (1) and (2), taking $\nu = 0.5$:

$$u_0 = \frac{\sigma_r + \sigma_\theta}{2} = \frac{F}{2\pi r_0}\left[\frac{r_0}{r} + \frac{2}{1+(R/r_0)^2}\frac{r}{r_0}\right]\cos\theta \tag{9}$$

During the consolidation process, the change in volumetric strain is linked to the change in mean effective stress by equation (8), and the latter may be assumed proportional to the change in excess pore pressure:

$$\frac{\partial s'}{\partial t} = -\frac{\chi}{2}\frac{\partial u_e}{\partial t} \tag{10}$$

where χ is a proportionality factor.

For one-dimensional consolidation with constant total vertical stress, it may be shown that the proportionality factor is $1/(1 - \nu)$. Here, however, we do not have conditions of constant total radial stress (although the radial stress at r_0 is essentially independent of Poisson's ratio).

The value of the proportionality factor χ can be evaluated by relating the change of the excess pore water during the consolidation stage to the change of the effective stresses. At the end of consolidation the excess pore pressure will be zero and the change in mean effective stress is

$$s' = \frac{F}{4\pi r_0}\frac{1}{(1-\nu)}\left[\frac{r_0}{r} + \frac{2}{(3-4\nu)}\frac{1}{1+(R/r_0)^2}\frac{r}{r_0}\right]\cos\theta \tag{11}$$

Over the complete consolidation period, comparing equations (9) and (11) and ignoring the second terms within the square brackets (given that $R >> r_0$), gives

$$\Delta s' \approx -\frac{1}{2(1-\nu)}\Delta u_e \tag{12}$$

Hence, just as in one-dimensional consolidation, we may take

$$\chi \approx \frac{1}{(1-\nu)} \tag{13}$$

Combining this result with equations (8) and (10) leads to:

$$\frac{\partial \varepsilon_v}{\partial t} = -\frac{(1-2\nu)}{2(1-\nu)G}\frac{\partial u_e}{\partial t} \tag{14}$$

Thus by substituting in equation (5)

$$\frac{\partial u_e}{\partial t} = c\nabla^2 u_e \tag{15}$$

where c is the consolidation constant given by:

$$c = \frac{2kG(1-\nu)}{(1-2\nu)\gamma_w} \tag{16}$$

This expression for c does indeed turn out to be identical to the usual one-dimensional consolidation coefficient, as suggested by Carter and Booker (1981); a similar result is found for purely radial consolidation around piles (Randolph and Wroth, 1979).

SOLUTION OF EQUATION FOR PORE WATER PRESSURE DISSIPATION

Equation (15) can be solved if it is assumed that the excess pore water pressure u_e can be expressed as a separate function of three variables t, r, and θ:

$$u_e = f_1(r).f_2(t).f_3(\theta) \tag{17}$$

Equations (9) and (10) suggest that $f_3(\theta)$ should be taken as $\cos\theta$, from which substitution of equation (17) into equation (15) leads to

$$f_1(r)\cos\theta\frac{\partial f_2(t)}{\partial t} = c\left[\frac{\partial^2 f_1(r)}{\partial r^2}.f_2(t).\cos\theta + \frac{f_2(t).\cos\theta}{r}\frac{\partial f_1(r)}{\partial r} - \frac{f_1(r)f_2(t)\cos\theta}{r^2}\right] \tag{18}$$

By re-arranging and eliminating cosθ:

$$\frac{1}{cf_2(t)}\frac{\partial f_2(t)}{\partial t}=\frac{1}{f_1(r)}\frac{\partial^2 f_1(r)}{\partial r^2}.+\frac{1}{rf_1(r)}\frac{\partial f_1(r)}{\partial r}-\frac{1}{r^2} \tag{19}$$

The left-hand side is now a function of t only and the right-hand side is a function of r alone. Therefore equation (19) can be re-written as two separate equations:

$$\frac{1}{cf_2(t)}\frac{\partial f_2(t)}{\partial t}=-\lambda^2 \tag{20}$$

and

$$\frac{1}{f_1(r)}\frac{\partial^2 f_1(r)}{\partial r^2}+\frac{1}{rf_1(r)}\frac{\partial f_1(r)}{\partial r}-\frac{1}{r^2}=-\lambda^2 \tag{21}$$

where λ is a constant.

The solution to equation (20) is:

$$f_2(t)=e^{-c\lambda^2 t} \tag{22}$$

while equation (21) can be re-written as:

$$\frac{\partial^2 f_1(r)}{\partial r^2}+\frac{1}{r}\frac{\partial f_1(r)}{\partial r}+\left(\lambda^2-\frac{1}{r^2}\right)f_1(r)=0 \tag{23}$$

the solution of which is a linear combination of first order Bessel functions of the first and of the second kind (McLachlan, 1955):

$$f_1(r)=A\left[J_1(\lambda r)+\alpha Y_1(\lambda r)\right] \tag{24}$$

Therefore the solution for u_e can be written as:

$$u_e=A\left[J_1(\lambda r)+\alpha Y_1(\lambda r)\right]e^{-c\lambda^2 t}\cos\theta \tag{25}$$

Since Bessel functions of first order are oscillating functions, there are an infinite number of values of the coefficients A, α, and λ that satisfy this equation. The full expression for u_e will involve a summation of all possible solutions:

$$u_e = \sum_{n=1}^{\infty} A_n \left[J_1(\lambda_n r) + \alpha_n Y_1(\lambda_n r) \right] e^{-c\lambda_n^2 t} \cos\theta \tag{26}$$

The boundary conditions around a rigid, impermeable pile are:

$$u_e = 0 \qquad \text{at } r = R \tag{27}$$

$$\frac{\partial u_e}{\partial r} = 0 \quad \text{at } r = r_0 \tag{28}$$

$$u_e = u_0 \quad \text{at } t = 0 \qquad \text{for } r_0 \le r \le R \tag{29}$$

Satisfying equation (27) implies that:

$$J_1(\lambda_n R) + \alpha_n Y_1(\lambda_n R) = 0 \tag{30}$$

so that the coefficient α_n is given by

$$\alpha_n = -\frac{J_1(\lambda_n R)}{Y_1(\lambda_n R)} \tag{31}$$

From the properties of Bessel functions (McLachlan, 1955):

$$\frac{\partial}{\partial r}\left[J_1(\lambda_n r) + \alpha_n Y_1(\lambda_n r) \right] = \frac{\lambda_n \left[J_2(\lambda_n r) - J_0(\lambda_n r) \right]}{2} + \alpha_n \frac{\lambda_n \left[Y_2(\lambda_n r) - Y_0(\lambda_n r) \right]}{2} \tag{32}$$

Substituting equation (31) into (32) and satisfying the boundary condition given by equation (28) gives:

$$Y_1(\lambda_n R)\left[J_2(\lambda_n r_0) - J_0(\lambda_n r_0) \right] - J_1(\lambda_n R)\left[Y_2(\lambda_n r_0) - Y_0(\lambda_n r_0) \right] = 0 \tag{33}$$

Thus, λ_n represents the non-zero roots of the cylindrical function given by equation (33). Once λ_n is found, α_n can be evaluated.

Satisfying the boundary condition at t = 0 (equation (29)) implies that:

$$\sum_{n=1}^{\infty} A_n \left[J_1(\lambda_n r) + \alpha_n Y_1(\lambda_n r) \right] \cos\theta = u_0 \tag{34}$$

Multiplying both sides of this equation by $r\left[J_1(\lambda_n r) + \alpha_n Y_1(\lambda_n r) \right]$, integrating between r_0 and R and using the orthogonal properties of Bessel functions, gives

$$\int_{r_0}^{R} r u_0 \left[J_1(\lambda_n r) + \alpha_n Y_1(\lambda_n r) \right] dr = \frac{A_n \cos\theta}{2} \left\{ \begin{array}{l} R^2 \left[\left(J_1(\lambda_n R) + \alpha_n Y_1(\lambda_n R) \right)^2 - \left(J_0(\lambda_n R) + \alpha_n Y_0(\lambda_n R) \right) \left(J_2(\lambda_n R) + \alpha_n Y_2(\lambda_n R) \right) \right] \\ - r_0^2 \left[\left(J_1(\lambda_n r_0) + \alpha_n Y_1(\lambda_n r_0) \right)^2 - \left(J_0(\lambda_n r_0) + \alpha_n Y_0(\lambda_n r_0) \right) \left(J_2(\lambda_n r_0) + \alpha_n Y_2(\lambda_n r_0) \right) \right] \end{array} \right\} \tag{35}$$

The values of A_n can then be found by integrating the left-hand side of equation (35).

DERIVATION OF EQUATION FOR DISPLACEMENTS DURING CONSOLIDATION

The stresses, strains, and displacements can be broken into transient and long-term

components. The transient components are time dependent and vary with the change in excess pore water pressure. The long-term components do not vary with time and can be calculated from the elastic solution. Thus, the radial displacement can be written as:

$$\rho_r = \rho_r^{\infty} + \rho_r^{t} \tag{36}$$

where the superscript ∞ donates the long-term component while t indicates the transient component, which is a negative quantity that reduces in magnitude to zero at large time.

The radial displacements are calculated from the integral of the radial strain:

$$\rho_r = \int_r^R \varepsilon_r dr \tag{37}$$

In order to evaluate this, information is needed regarding the changes in σ'_r and σ'_θ, in addition to the change in s' (now known from equations (12) and (26)). Let us assume that:

$$\begin{aligned} \frac{\partial \sigma_r^{'}}{\partial t} &= 2\beta \frac{\partial s'}{\partial t} = -\frac{\beta}{(1-\nu)} \frac{\partial u_e}{\partial t} \\ \frac{\partial \sigma_\theta^{'}}{\partial t} &= 2(1-\beta) \frac{\partial s'}{\partial t} = -\frac{(1-\beta)}{(1-\nu)} \frac{\partial u_e}{\partial t} \end{aligned} \tag{38}$$

where β is a constant ($0 \le \beta \le 1$).

Substituting this into equation (6), the transient component of the radial strain can be written as:

$$\varepsilon_r^t = -\frac{(\beta - \nu)}{2(1-\nu)G} u_e \tag{39}$$

from which the transient component of the radial displacement may be derived as:

$$\rho_r^t = -\frac{(\beta-\nu)\cos\theta}{2(1-\nu)G}\sum_{n=1}^{\infty} e^{-c\lambda_n^2 t}\int_r^R A_n\left[J_1(\lambda_n r)+\alpha_n Y_1(\lambda_n r)\right]dr \qquad (40)$$

Hence

$$\rho_r^t = -\frac{(\beta-\nu)\cos\theta}{2(1-\nu)G}\sum_{n=1}^{\infty}\frac{A_n e^{-c\lambda_n^2 t}}{\lambda_n}\left(\left[J_0(\lambda_n r)+\alpha_n Y_0(\lambda_n r)\right]-\left[J_0(\lambda_n R)+\alpha_n Y_0(\lambda_n R)\right]\right) \qquad (41)$$

Combining this with equation (4), the general expression for the total radial displacement is therefore:

$$\begin{aligned}\rho_r = {} & \frac{F}{16\pi G}\frac{1}{(1-\nu)}\left[(3-4\nu)\ln\left(\frac{R}{r}\right)^2-\left(\frac{r_0}{r}\right)^2\frac{R^2-r^2}{R^2+r_0^2}-\frac{(4\nu-1)}{(3-4\nu)}\frac{R^2-r^2}{R^2+r_0^2}\right]\cos\theta \\ & -\frac{(\beta-\nu)\cos\theta}{2(1-\nu)G}\sum_{n=1}^{\infty}\frac{A_n e^{-c\lambda_n^2 t}}{\lambda_n}\left(\left[J_0(\lambda_n r)+\alpha_n Y_0(\lambda_n r)\right]-\left[J_0(\lambda_n R)+\alpha_n Y_0(\lambda_n R)\right]\right)\end{aligned} \qquad (42)$$

The pile displacement at t=0 can be estimated from the elastic solution by putting ν=0.5 in equation (4). Therefore, β can be shown to be given by:

$$\beta = \frac{\frac{F}{8\pi}\left((1-2\nu)\ln\left(\frac{R}{r_0}\right)^2-\frac{2}{(3-4\nu)}\frac{R^2-r_0^2}{R^2+r_0^2}+4(1-\nu)\frac{R^2-r_0^2}{R^2+r_0^2}\right)}{\sum_{n=1}^{\infty}\frac{A_n}{\lambda_n}\left(\left[J_0(\lambda_n r_0)+\alpha_n Y_0(\lambda_n r_0)\right]-\left[J_0(\lambda_n R)+\alpha_n Y_0(\lambda_n R)\right]\right)}+\nu \qquad (43)$$

It should be noted that the rate of change of radial effective stress with time is expected to be greater than the rate of change of circumferential effective stress, implying that $\beta > 0.5$. If the radial total stress were to remain constant, the rate of change of the radial

effective stress would equal the rate of change of the excess pore water pressure, implying an upper limit for β of (1 - ν).

The lateral displacement of the pile due to consolidation can be expressed in a non-dimensional form such as that suggested by Carter and Booker (1981):

$$U = \frac{\rho_r - (\rho_r)_{t=0}}{(\rho_r)_{t=\infty} - (\rho_r)_{t=0}} \tag{44}$$

where U is the degree of displacement. Substituting the expression for radial displacement into this gives

$$U = 1 - \frac{\sum_{n=1}^{\infty} \frac{A_n e^{-c\lambda_n^2 t}}{\lambda_n} \left(\left[J_0(\lambda_n r) + \alpha_n Y_0(\lambda_n r) \right] - \left[J_0(\lambda_n R) + \alpha_n Y_0(\lambda_n R) \right] \right)}{\sum_{n=1}^{\infty} \frac{A_n}{\lambda_n} \left(\left[J_0(\lambda_n r) + \alpha_n Y_0(\lambda_n r) \right] - \left[J_0(\lambda_n R) + \alpha_n Y_0(\lambda_n R) \right] \right)} \tag{45}$$

Thus, the degree of displacement of displacement does not depend on β.

VALIDATION

Any analytical solution for the soil consolidation around a laterally loaded pile must be applied over a wide range of pile geometries and soil stiffness. It is helpful to form dimensionless groups of relevant parameters, rather than investigate how the solution is affected by the variation of each individual soil parameter. Following the technique of dimensional analysis, the radial displacement at any fixed location can be expressed as:

$$\frac{\rho_r}{r_0} = f_4\left(\frac{F}{Gr_0}, \nu, \frac{R}{r_0}, \frac{ct}{r_0^2} \right) \tag{46}$$

where the final group is the usual non-dimensional factor T (Soderberg, 1962).

Since the displacement is proportional to the load for elastic conditions, the groups containing F and ρ_r can be combined to give:

$$\frac{\rho_r G}{F} = f_5\left(\nu, \frac{R}{r_0}, T\right) \tag{47}$$

The excess pore water at any fixed location can be expressed as:

$$\frac{u_e r_0}{F} = f_6\left(\nu, \frac{R}{r_0}, T\right) \tag{48}$$

Similarly the incremental effective stress can be expressed as:

$$\frac{\Delta\sigma' r_0}{F} = f_7\left(\nu, \frac{R}{r_0}, T\right) \tag{49}$$

Finite element analyses were carried out to provide data to validate the analytical solution derived in the previous sections. The parameters used in the FE analysis and the FE results will be presented in terms of the dimensionless groups shown above.

2D FE models

Two-dimensional plane-strain coupled stress-pore pressure finite element analyses were conducted using ABAQUS (HKS 2002) to investigate the response of a pile segment in a porous linear elastic soil subjected to a lateral load. The soil was modelled using eight-node plane-strain consolidation elements. Because of the symmetry, only half of the problem was modelled. Since the analytical analysis assumes a rigid pile, the stiffness of the pile was taken to be 10^6 times the stiffness of the soil. The soil and the pile were assumed to be fully bonded to be consistent with the assumption used in the elastic

solution of Baguelin et al. (1977). Smaller elements were used near the pile where the changes of stresses and strains are significant. The far field boundary was assumed to be fully fixed and displacements normal to the line of symmetry were prevented. The FE mesh consisted of 936 elements and 2950 nodes, with details of the finite element mesh shown in Figure 2. Two sets of analyses were conducted with different geometries and material properties (Table 1).

Each FE analysis was carried out in two steps. In the first step, a load was applied and no drainage was allowed across the boundaries of the mesh. This step establishes the initial distribution of the excess pore pressures which will be dissipated during the second step. During the second step, drainage was allowed to occur through the far-field boundaries. This was specified by prescribing the excess pore pressure at all nodes on this boundary to be zero. The analyses were carried out at different time increments until the excess pore water pressure dissipated. The reference stresses and the pore water pressure before applying the load in the initial step were taken to be zero.

The finite element results can be influenced by the discretisation of the mesh. Since the reference stresses at the beginning of the analysis are taken to be zero, the effective stresses therefore become equal to the total stresses by the end of the consolidation stage once the pore water pressures reduce to zero. Thus, the elastic solution of Baguelin et al. (1977) can be used to check the accuracy of the finite element discretisation. Figure 3 shows that the stresses in the radial and circumferential directions and the radial displacements along a centreline path in the direction of the load, as calculated from

equations (1), (2) and (4), are consistent with those predicted by the finite element.

Stresses and excess pore water pressure at t = 0

Figure 4 shows the effective radial and circumferential stresses at points located between the pile circumference and the outer boundary of the deformable soil along the direction of the pile loading ($\theta = 0°$). The stresses are calculated immediately after applying the lateral load and before the pore water pressure starts to dissipate ($t = 0$). Figure 4 shows that the incremental effective radial and circumferential stresses generated in undrained conditions are equal in magnitude but opposite, giving zero change in mean effective stress as anticipated. $\Delta\sigma'_r$ and $\Delta\sigma'_\theta$ are zero adjacent to the pile. Both $\Delta\sigma'_r$ and $\Delta\sigma'_\theta$ have a peak value at a radial distance of about $1.75r_0$ from the centre of the pile. After the peak, the incremental effective stresses decrease gradually to a zero value at the boundary of the deformable soil. Figure 4 demonstrates that the radial and the circumferential stresses from the FE analyses before the pore water pressure starts to dissipate can be replicated analytically. In the analytical solution the effective stresses are calculated by subtracting the initial pore water pressure, calculated from equation (9), from the total stresses, calculated from equations (1) and (2) with $\nu = 0.5$.

Figure 5 shows the excess pore water pressure generated by the pile load in undrained conditions calculated from the FE analysis and that predicted from equation (9) assuming that the excess pore water pressure is equal to the total stress increment. The analytical values are in excellent agreement with the FE results. It can be seen from the results plotted in Figure 5 that there is a unique excess pore water pressure distribution near the

pile regardless of the size of the deformable soil zone. Away from the pile the values of the initial excess pore water pressure depend on R/r_0.

Dissipation of excess pore water pressure with time

Figure 6a shows the variation of excess pore water pressure in the circumferential direction in the soil adjacent to the pile at different non-dimensional time factors. The results are obtained from the FE analysis using the Set 1 parameters. Figure 6b re-plots the data as excess pore water pressure normalized by the value at $\theta = 0°$. This figure illustrates clearly that the distribution of the excess pore water pressure in the circumferential direction follows a cosine function throughout the consolidation process as proposed in equation (26).

Figure 7 shows the variation of the excess pore water pressure with time factor T for a point adjacent to the pile ($r = r_0$) located in the direction of the load ($\theta = 0°$), for the two sets of the parameters given in Table 1. The excess pore water pressure is calculated using equation (26) and is normalized by its initial value which is calculated from equation (9). The calculations are carried out for the two different sizes of assumed soil deformation zones, $R/r_0 = 60$ (Figure 7a) and $R/r_0 = 25$ (Figure 7b). A summation of 11268 terms of equation (26) was used to plot the analytical results in Figure 7a. This number of terms corresponds to the number of non-zero roots λ_n of equation (33) for values of λr_0 between 0 and 600. This number of terms gives insignificant error of 0.1619% for the value of the initial excess pore water pressure (at $t = 0$ and $r = r_0$) calculated using equation (9). For the results shown in Figure 7b, 7639 terms were used

and the corresponding error was 0.3811%. The number of terms corresponds to the non-zero roots of equation (33) for values of λr_0 between 0 and 1000.

Both the analytical calculations in Figures 7a and 7b are in excellent agreement with the finite element results. The results plotted in Figure 7 show that about 90% of the excess pore water pressure dissipated by a time factor $T \sim 5$. About 99% of the excess pore water pressure dissipated by $T \sim 50$.

The analytical curves shown in Figure 7a and 7b are almost identical. Therefore, it can be concluded that the relation between the normalized excess pore water pressure and the non-dimensional time factor T is independent of the assumed size of the deformable zone (i.e. the radius R).

Displacement prediction

Figure 8 shows the pile displacement calculated from the finite element analysis and that predicted using equation (42). The values of β calculated from equation (43) are 0.6398 and 0.5752 respectively for the two parameter set. The analytical solution gives reasonable displacement prediction. However, it should be noted that substitution of $\nu = 0.5$ in equation (4) gives values of $\rho_r G/F$ of 0.246 and 0.177 respectively for the two parameter sets, and these values are slightly lower than the true undrained displacements.

Figure 9 shows the results shown in Figure 8 re-plotted as the degree of consolidation displacement U against the non-dimensional time factor T. The analytical solution is

calculated using equation (45). The finite element results plot to the right of the analytical solution, which therefore slightly overestimates the degree of consolidation displacement for any given value of T.

Figure 9 indicates that the degree of consolidation displacement for a given value of T varies with R/r_0. Further insight into this can be obtained by plotting just the transient component of displacement, non-dimensionalised as $\Delta\rho_r G/F$, as shown in Figure 10. It may be seen that the consolidation displacement follows approximately a unique curve, independent of R/r_0 (apart from a slight variation for the extreme value of $R/r_0 = 10$), until the limiting value is reached, but that the limiting value itself depends on R/r_0.

COMPARISON WITH 3D ANALYSIS

The analysis and results presented here are based on conditions of plane strain. In the true three-dimensional case of a laterally loaded pile, drainage can occur towards the ground surface at shallow depths. The surface drainage will therefore accelerate the consolidation process at shallow depths. In order to examine the three-dimensional effects, 3D finite element analysis was carried out. The three-dimensional finite element mesh is shown in Figure 11, and represents a semi-cylindrical section through a diametrical plane of a pile of radius r_0 and a length L equal to $20r_0$. The radius of the mesh is equal to $25r_0$ and the depth of the mesh is equal to $30r_0$. Displacement boundary conditions prevent out-of-plane displacements of the vertical boundaries (that is, the flat diametrical plane on the front face of the mesh, and around the circumference), and the base of the mesh is fixed in all three coordinate directions. The finite element mesh comprises 10,484 second-order

continuum hexahedral (brick) elements with a total of 46,374 nodes. The stiffness of the pile was taken to be 10^6 times the stiffness of the soil. The soil and the pile were assumed to be fully bonded. Smaller elements were used near the pile where the changes of stresses and strains are significant.

The 3D FE analysis was carried out with a Poisson's ratio ν of 0.2 and F/G r_0 of 0.48, with the horizontal force F is applied at the top of the pile (i.e. at the ground surface). During the consolidation step of the analysis, drainage was allowed to occur through the far-field vertical boundaries at circumference of the mesh (i.e. in the radial direction) and through the free surface.

Figure 12 compares the degree of displacement of the pile head from the three-dimensional finite element analysis compared with the two-dimensional analytical solution. The 3D finite element results are similar to those obtained by Taiebat and Carter (2001) using a discrete Fourier finite element approach. However, it should be noted that in Taiebat and Carter (2001) drainage was allowed to occur only at the free surface. It may be seen from the figure that the present solution under-predicts the degree of consolidation in respect of the pile head displacement unless surface drainage is eliminated (by a pile cap for example). Nevertheless, it remains useful to estimate the duration of the consolidation process.

Figure 13 shows the FE results of the decay of the excess pore water pressure during the consolidation at all the nodes at the soil-pile interface at normalized depth z/L between

0.05 and 0.7. The excess pore water pressure is normalized by its initial value. This figure shows that the 2D analytical solution can reasonably predict the consolidation process along the shaft of the pile. However, it cannot predict the consolation of soils near the tip of the pile or near the ground surface. As can be seen from the displacement vectors shown in Figure 14, the vertical displacements around a laterally loaded pile at the end of consolidation are significantly smaller compared with the horizontal displacements. Therefore, the 2D analysis is justified.

CONCLUSIONS

A closed form solution for the variation of the excess pore water pressure with time around a laterally loaded pile has been derived. The solution is based on a two-dimensional plane-strain idealisation with the soil taken to be a porous linear elastic material. In this solution, drainage is assumed to occur at the boundary of the assumed zone of deformable soil around the pile. The analytical solution has been validated against results from coupled consolidation finite element analysis.

An expression for the initial excess pore water pressure generated immediately after the application of the load and before the start of consolidation was derived from the elastic solution of Baguelin et al. (1977) assuming incompressible conditions. This prediction is shown to be in excellent agreement with the finite element results.

It was found that there is a unique relation between the excess pore water pressure

normalised by its initial value and the non-dimensional time factor $T = ct/r_0^2$ where c is the conventional one-dimensional consolidation coefficient. This relationship does not depend on the assumed radius of the deformable zone or the soil properties.

A closed form solution for the variation of the pile displacement with time was obtained. The accuracy of this solution requires estimation of the relationship between the rate of change of radial effective stress and the excess pore water pressure. Guidelines on how to estimate this relationship are given and illustrated.

The solution is based on plane-strain assumptions. Comparison with three-dimensional analysis of a laterally loaded pile shows that the degree of consolidation is slightly under-predicted because of effects such as drainage towards the free surface.

The solution for consolidation around an embedded cylinder in a porous medium, which is presented here, has potential for applications in a variety of geotechnical problems. Consolidation around T-bar penetrometers and around deeply embedded pipelines are among the possible applications of this solution.

REFERENCES

Baguelin, F, Frank, R, Said, Y.H. (1977). Theoretical study of lateral reaction mechanism of piles. Geotechnique 27(3): 405-434.

Biot, M.A. (1941). General theory of three-dimensional consolidation. *Journal of Applied Physics*, 12, 155–164.

Carter, J.P, Booker, J.R. (1981). Consolidation due to lateral loading of a pile. Proceedings of the 10th International conference on soil mechanics and foundation engineering, International conference on soil mechanics and foundation engineering, 10, Stockholm,, Vol. 2, pp. 647-650

Hetenyi, M. (1946). *Beams on elastic foundations.* Ann Arbor: University of Michigan Press.

Hibbit, Karlsson & Sorensen Inc. (2003). ABAQUS/Standard User's manual, version 6.5.

Poulos, H.G. (1971a). Behaviour of laterally loaded piles: 1, single piles. *Journal of Soil Mechanics. Foundation Engineering Division.,* American Society of Civil Engineers. 97(5): 711-731.

Krost K., Gourvenec S. and White D. J. Consolidation around partially embedded seabed pipelines. Géotechnique (in print, published online on 08 July 2010).

Matlock, H. and Reese, L.C. (1960). Generalised solutions for laterally loaded piles. *Journal Soil Mechanics and Foundation Division,,* American Society for Civil Engineers (86)5: 63–91.

McLachlan N.W. (1955), Bessel Functions for Engineers. Oxford, Clarendon Press.2nd edition.

Mindlin, R.D. (1936). Force at a point in the interior of a semi-inlinite solid. *Physics 7*, 195-202.

Mylonakis, G. (2001). Winkler modulus for axially loaded piles. Geotechnique 51(5): 455-461.

Osman, A.S and Randolph, M. F. 2010. Response of a solid infinite cylinder embedded in a poroelastic medium and subjected to a lateral load. *International Journal of Solids and Structures* 47(18-19): 2414-2424.

Randolph, M.F. (1981). Response of flexible piles to lateral loading. Geotechnique 31(2): 247-259.

Randolph, M.F, Wroth, C.P. (1979). Analytical solution for the consolidation around a driven pile. International Journal for Numerical and Analytical Methods in Geomechanics, 3(3):217-229.

Shirazi A. and Selvadurai A. P. S. (2005). Lateral loading of a rigid rock socket embedded in a damage-susceptible poroelastic solid. International Journal of Geomechanics

5(4): 276-285.

Soderberg, L.O. (1962). Consolidation theory applied to foundation pile time effects. Geotechnique 12(3):217-225.

Taiebat H.A. and Carter J.P. (2001). A semi-analytical finite element method for three-dimensional consolidation analysis. Computer and Geotechnics 28(1):55-78

Terzaghi, K., Die Berechnung der Durchlässigkeitsziffer des Tones aus dem Verlauf der hydrodynamischen Spannungserscheinungen. *Sitzungsber. Akad. Wiss. Wien. Math-Naturwiss. Kl., Part Iia*, 1923, 32, 125–138.

Winkler, E. (1867). *Die Lehre van Elastizitiit und Festigkeit.* Prague.

	$\frac{F}{Gr_0}$	ν	$\frac{R}{r_0}$
Set 1	0.48	0.2	60
Set 2	0.14	0.4	25

Table 1 Parameters used in the FE analysis

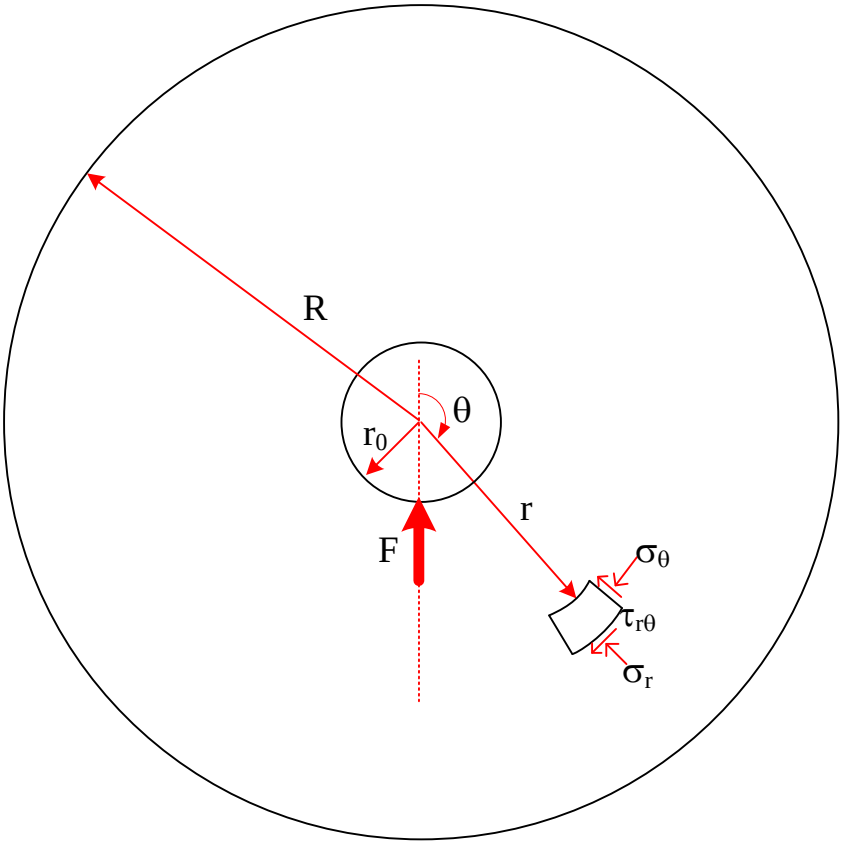

Figure 1 Nomenclature for pile under lateral load

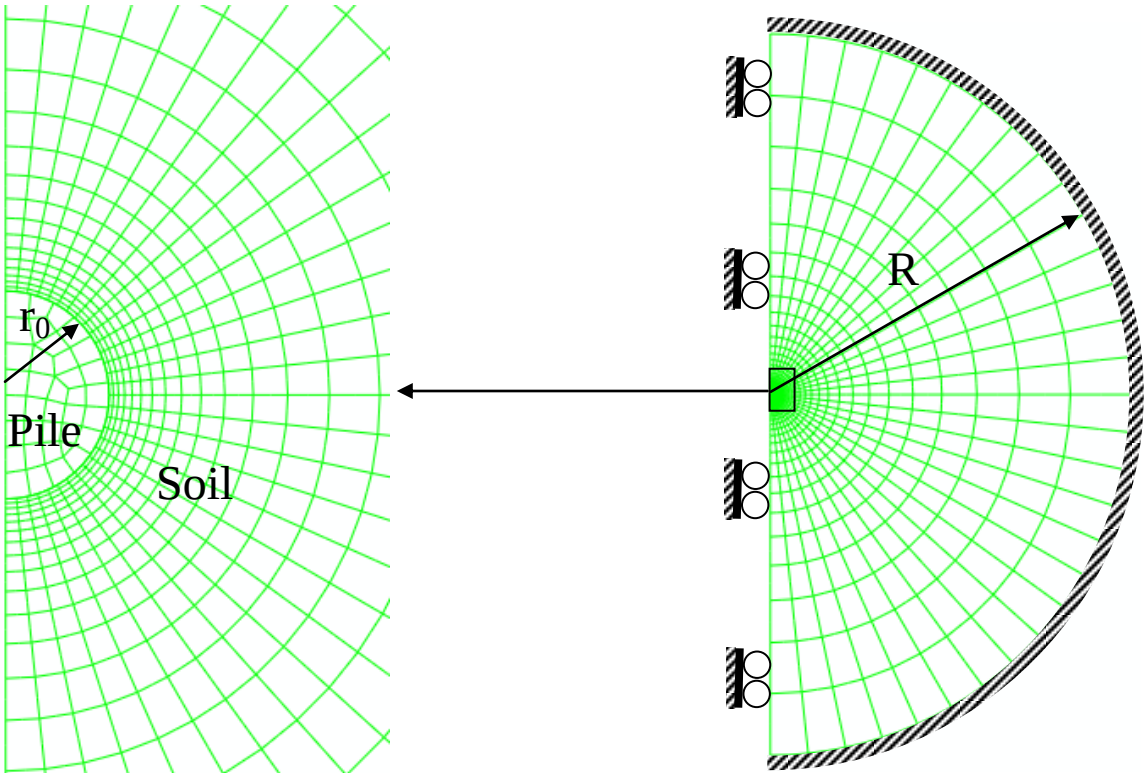

Figure 2 2D finite element mesh

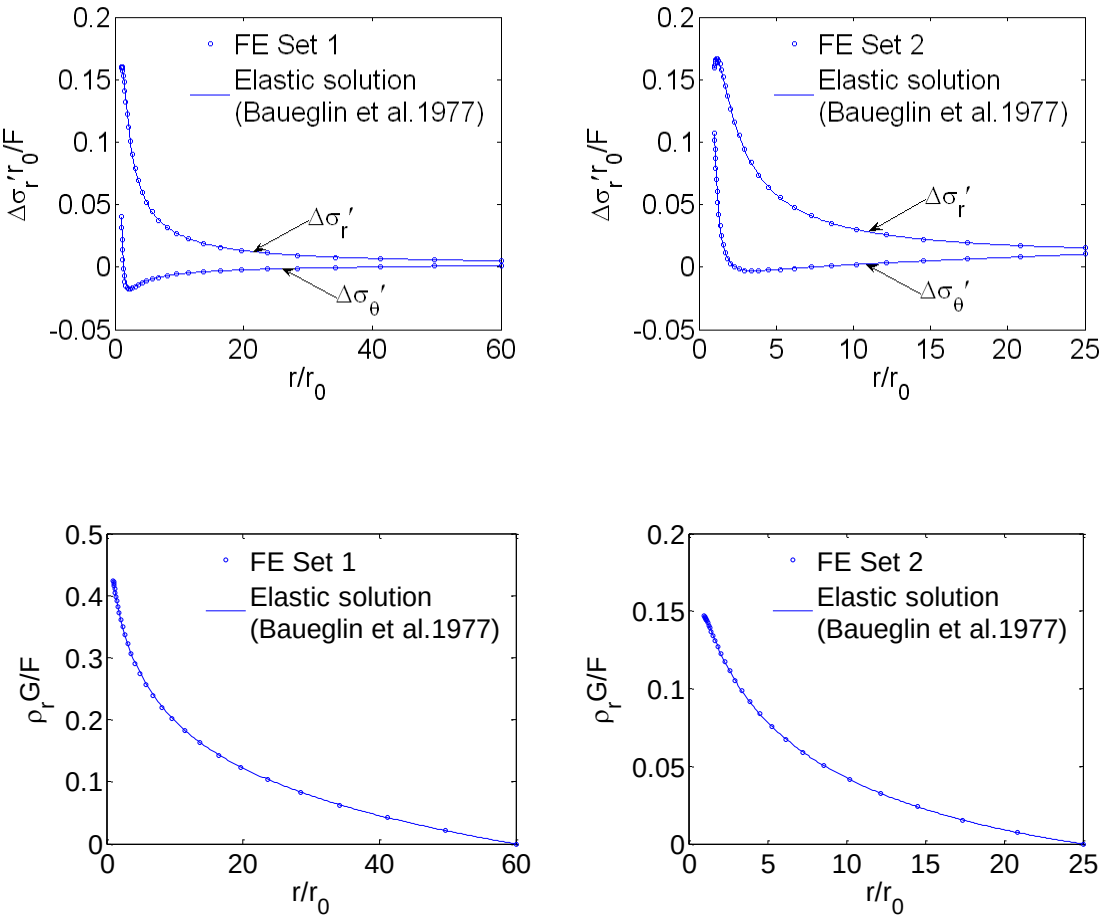

Figure 3 Accuracy of the finite element mesh: comparison with elastic solution at the steady state (after the dissipation of the excess pore water pressure)

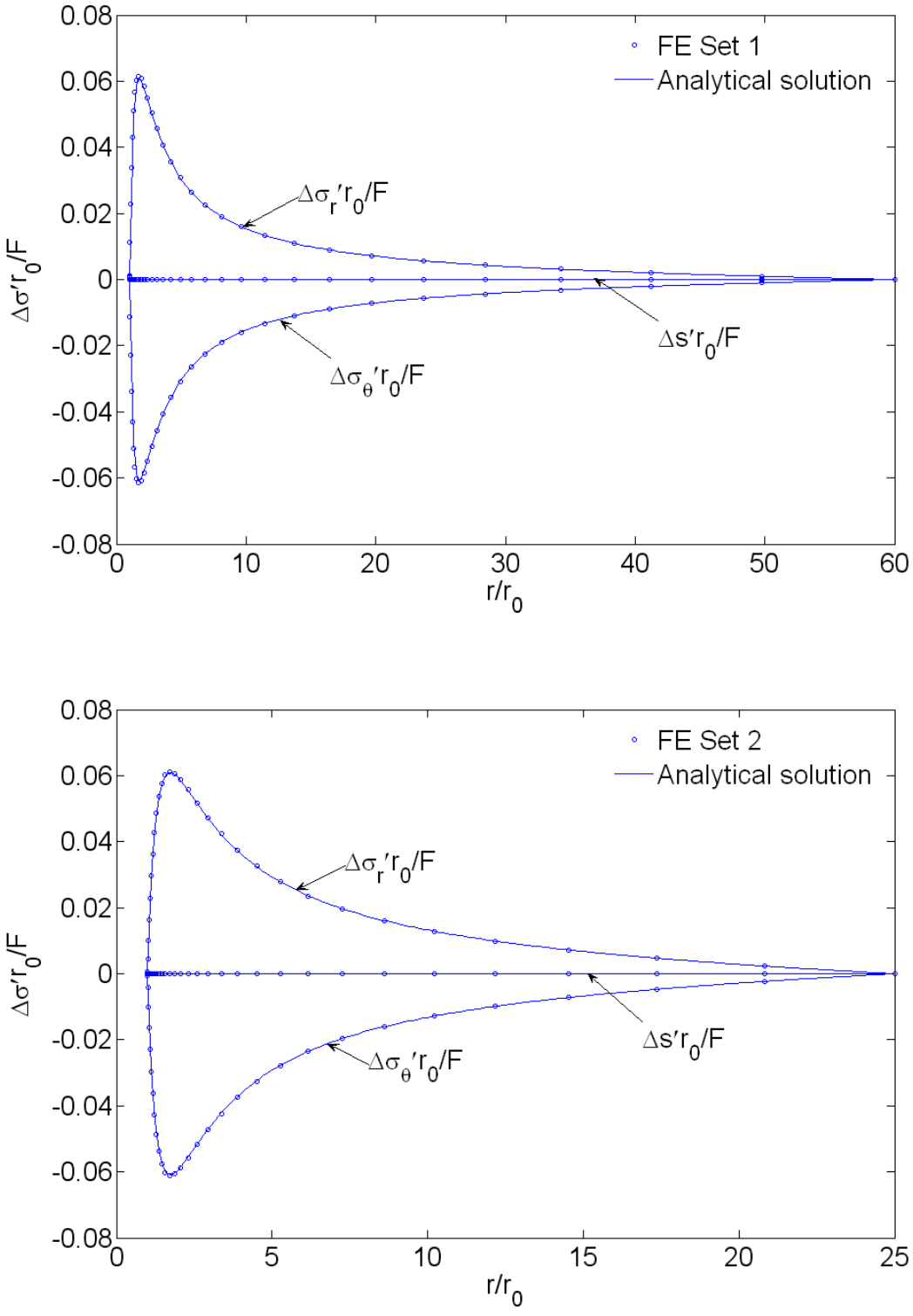

Figure 4 Effective stresses before the excess pore water pressure starts to dissipate

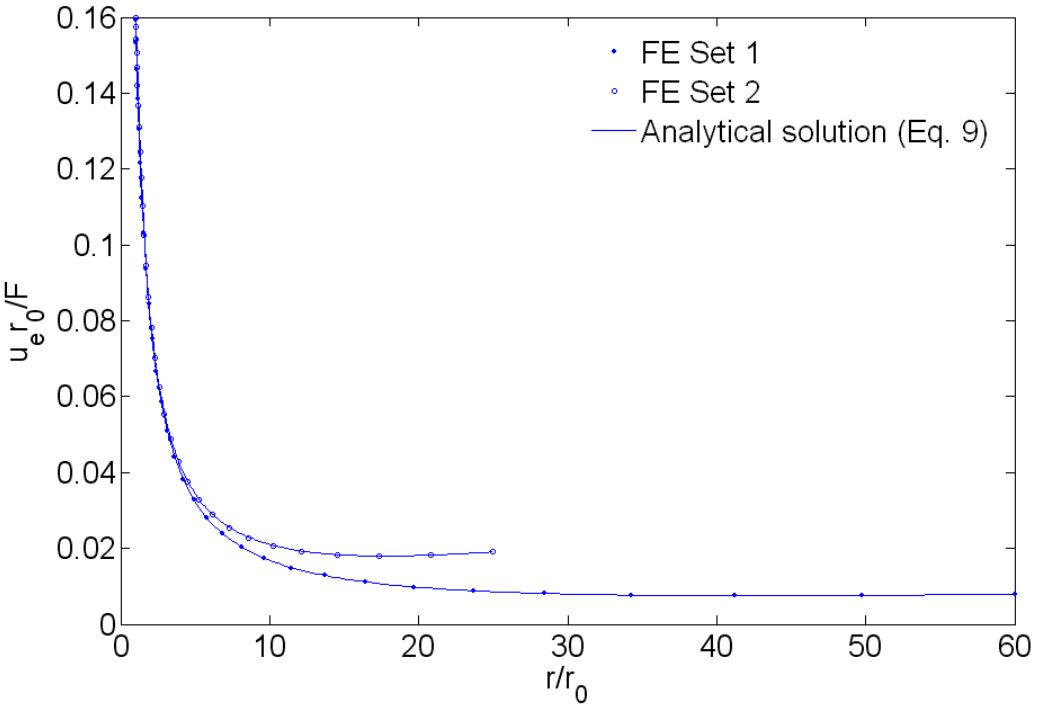

Figure 5 Initial excess pore water pressure distribution along a path in the direction of the lateral load (θ=0°)

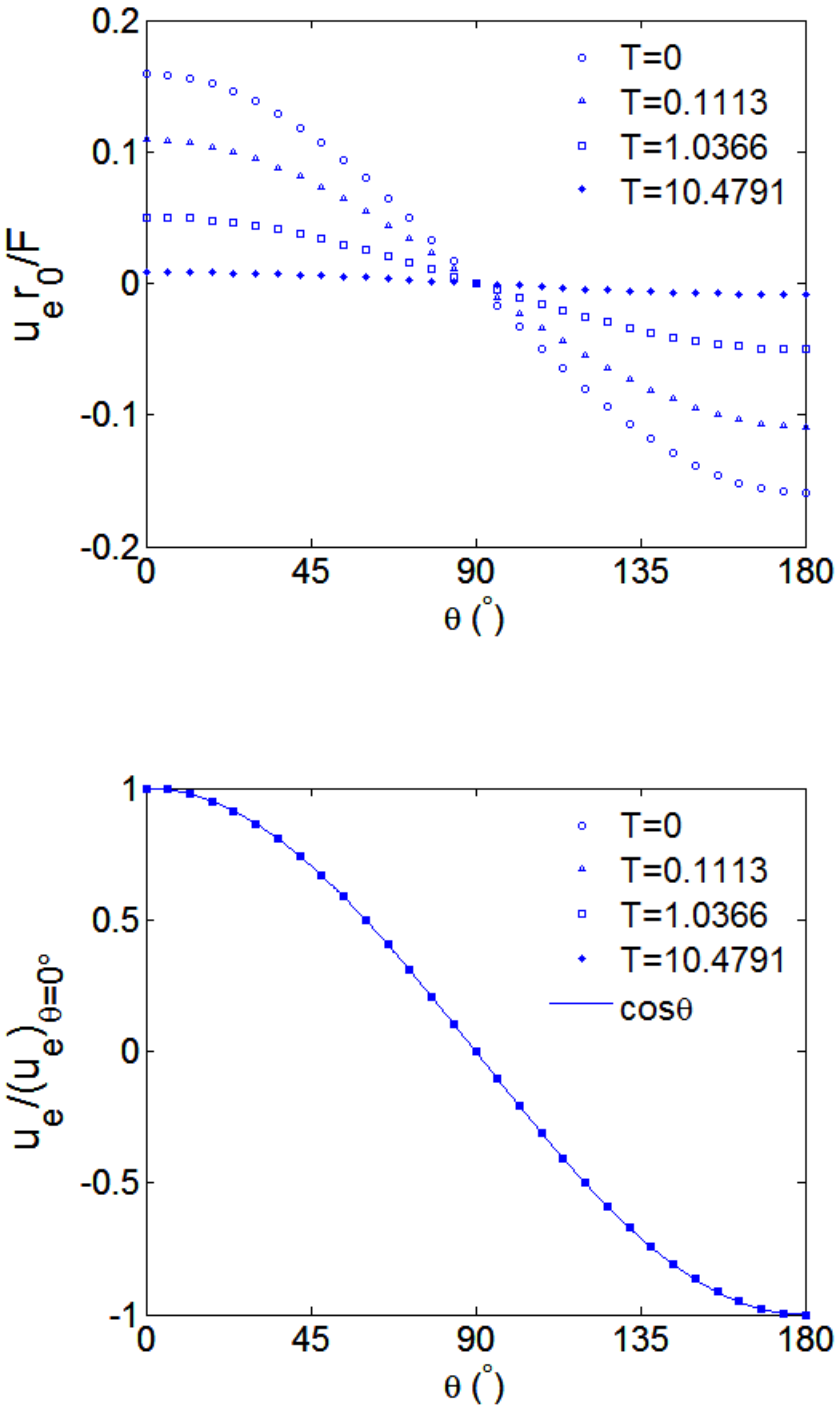

Figure 6 Variation of excess pore water pressure in the circumferential direction ($r=r_0$)

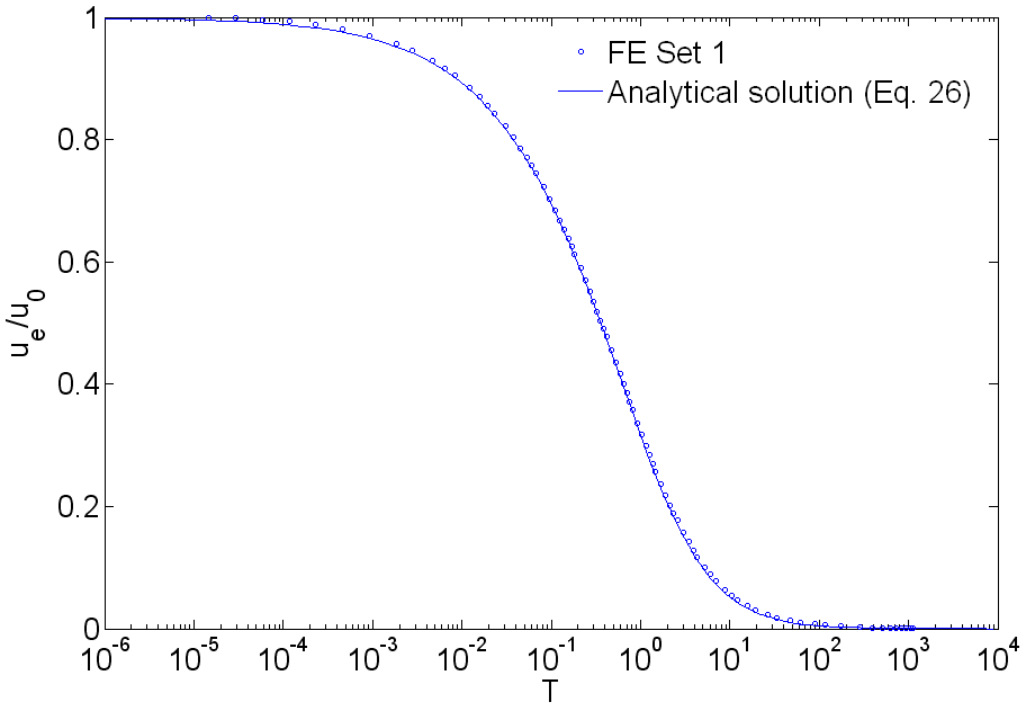

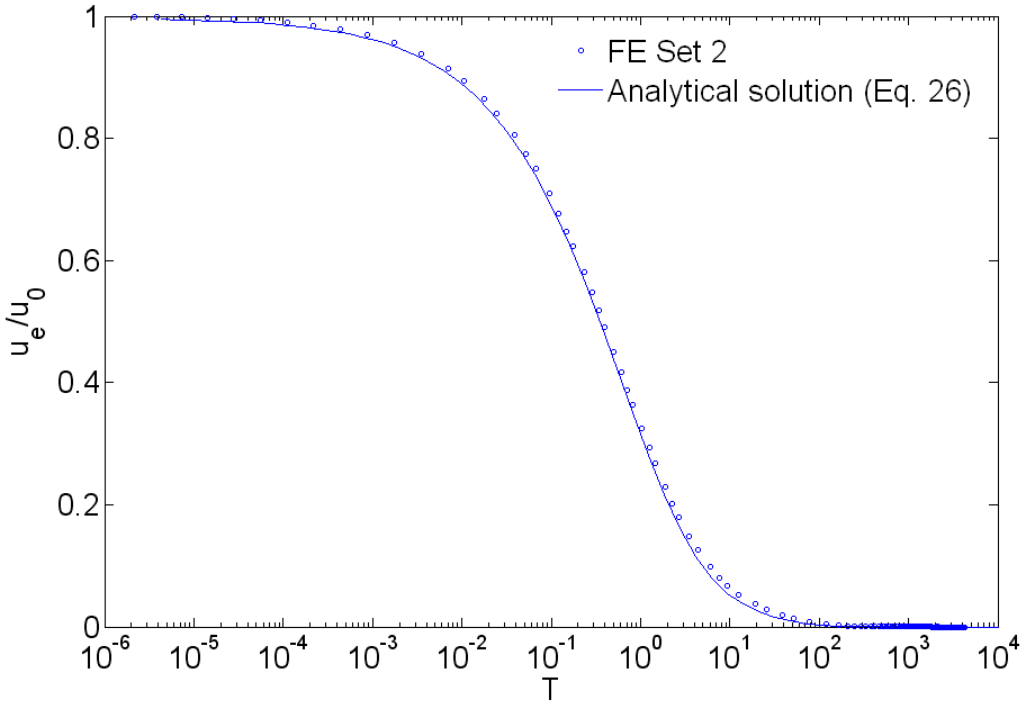

Figure 7 Decay of excess pore water pressure with time

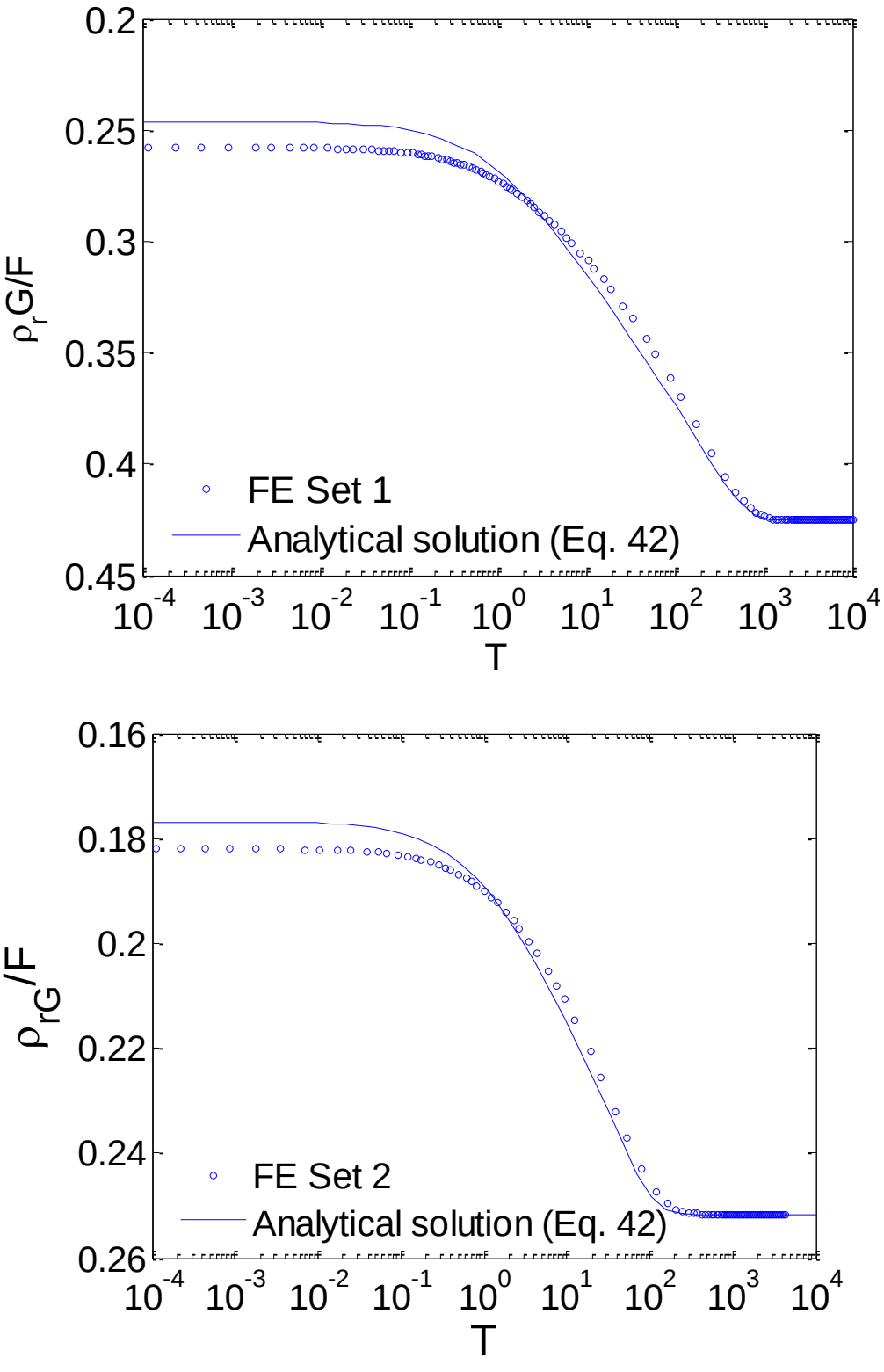

Figure 8 Variation of pile displacement with time

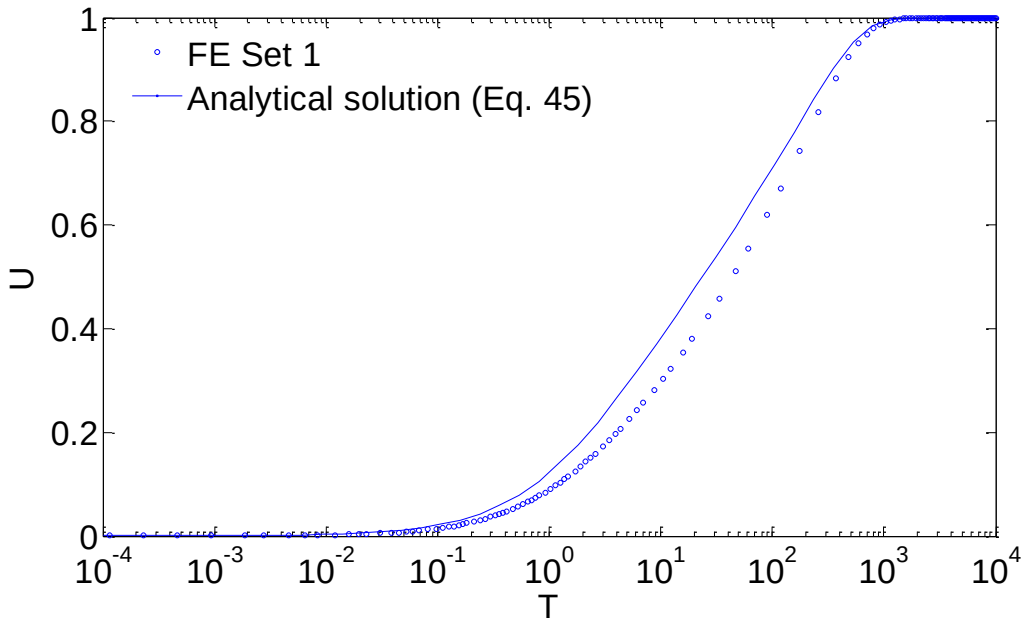

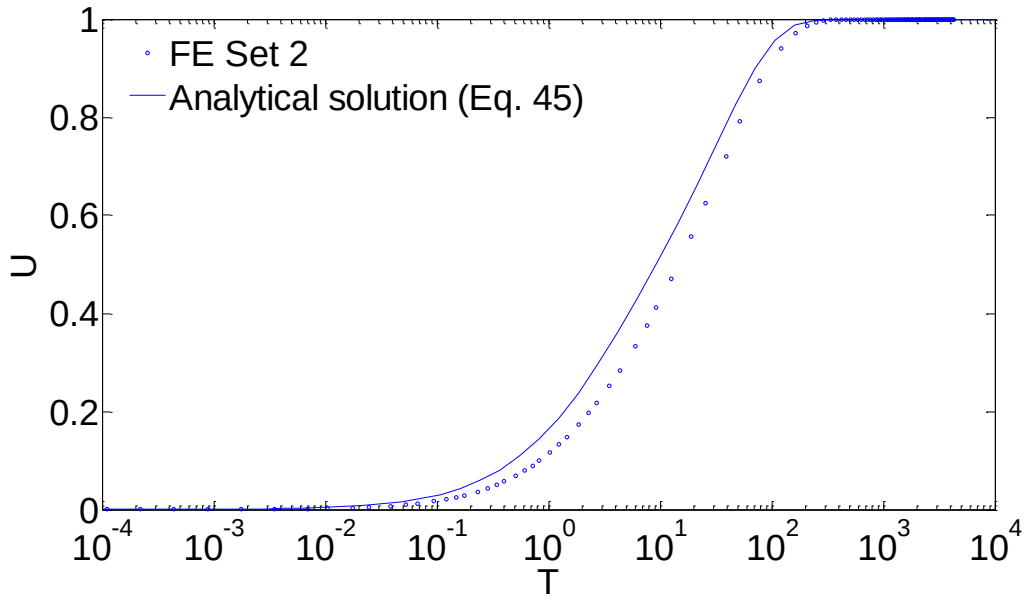

Figure 9 Variation of the degree of pile displacement with time

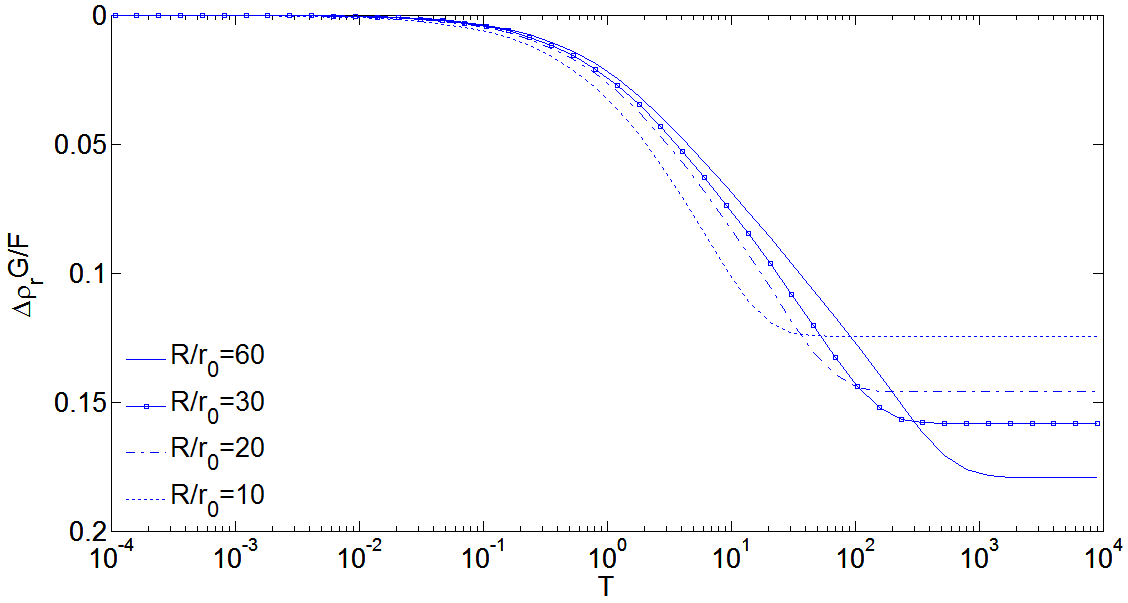

Figure 10 Variation of the pile consolidation displacement with time

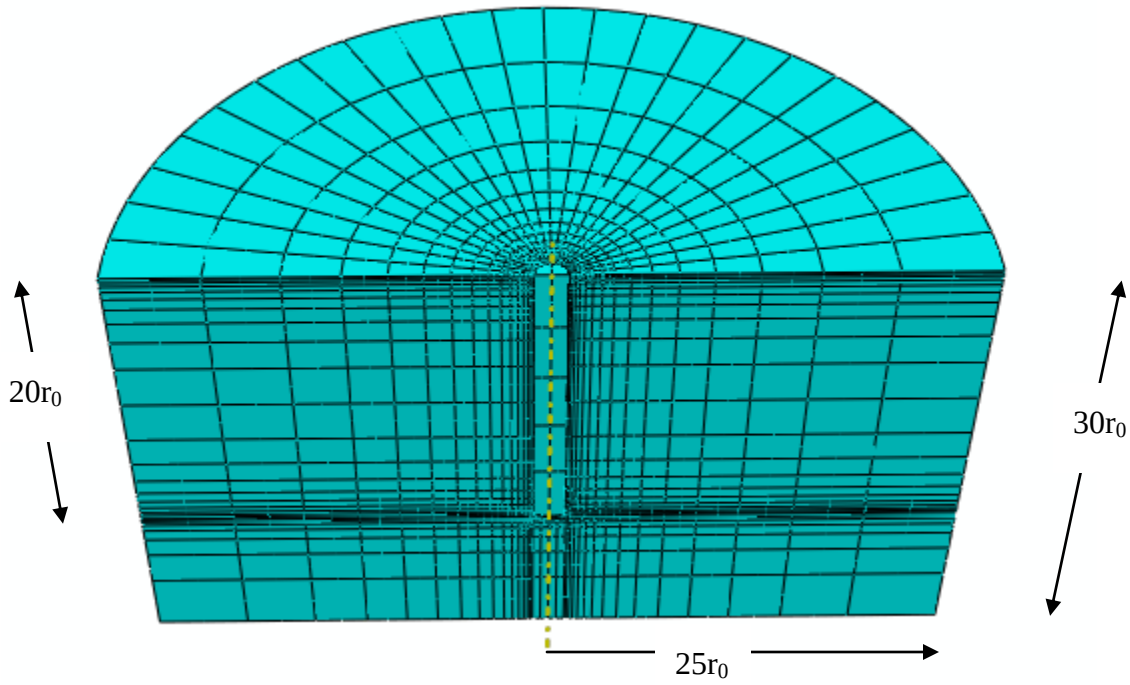

Figure 11 3D finite element mesh

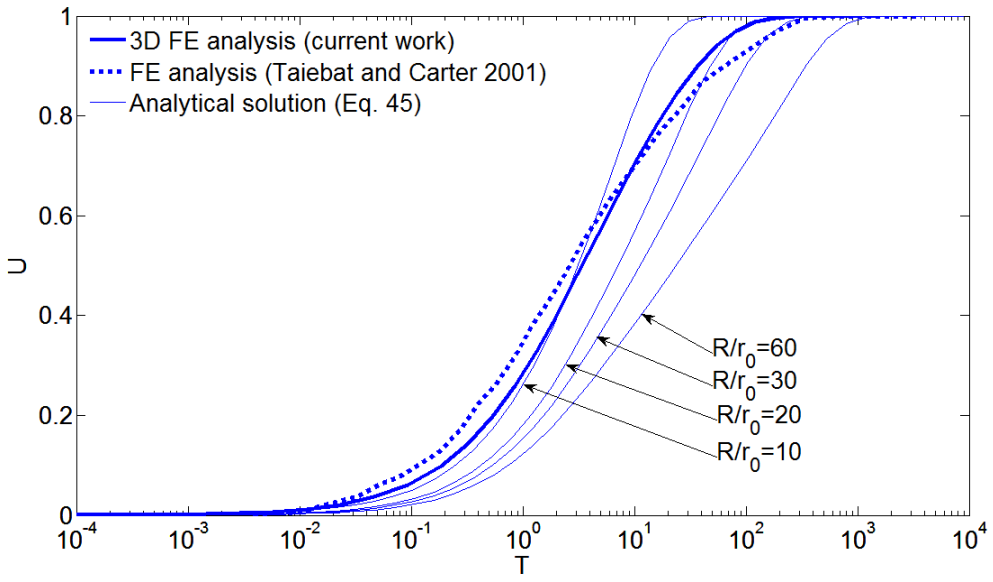

Figure 12 Effect of 3-dimensional consolidation on the displacement of the pile head

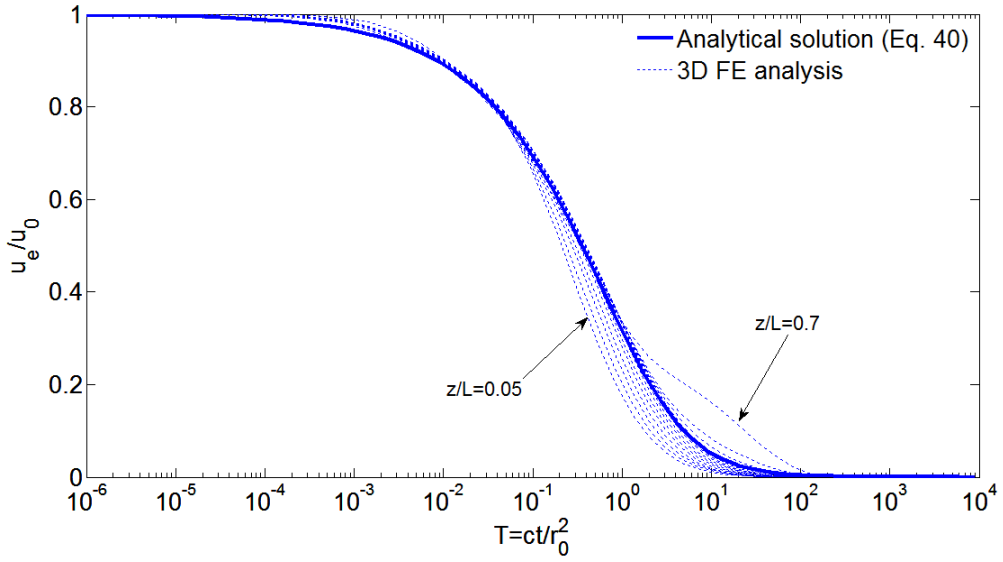

Figure 13 Decay of excess pore water pressure with time along the shaft of the pile (z/L=0.05~0.70)

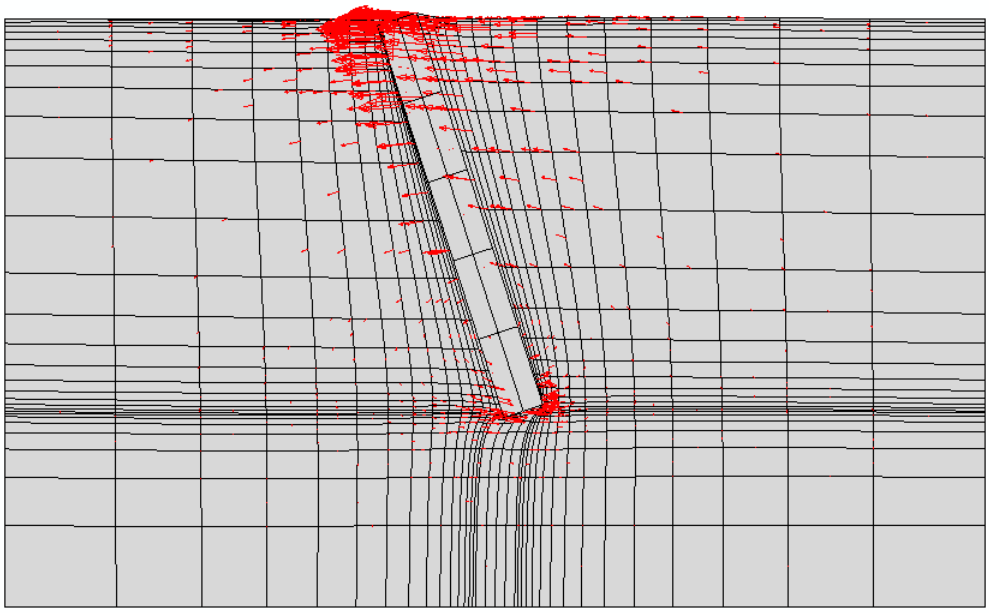

Figure 14 Displacement vectors at the end of the consolidation process (note: magnitude of displacements is not to scale)